nature energy

ARTICLES

https://doi.org/10.1038/s41560-017-0018-7

A flexible metal–organic framework with a high density of sulfonic acid sites for proton conduction

Fan Yang[1], Gang Xu[2], Yibo Dou[1], Bin Wang[1], Heng Zhang[1], Hui Wu[3], Wei Zhou[3], Jian-Rong Li[1]* and Banglin Chen[4,5]*

The design of stable electrolyte materials with high proton conductivity for use in proton exchange membrane fuel cells remains a challenge. Most of the materials explored have good conductivity at high relative humidity (RH), but significantly decreased conductivity at reduced RH. Here we report a chemically stable and structurally flexible metal–organic framework (MOF), BUT-8(Cr)A, possessing a three-dimensional framework structure with one-dimensional channels, in which high-density sulfonic acid (–SO_3H) sites arrange on channel surfaces for proton conduction. We propose that its flexible nature, together with its –SO_3H sites, could allow BUT-8(Cr)A to self-adapt its framework under different humid environments to ensure smooth proton conduction pathways mediated by water molecules. Relative to other MOFs, BUT-8(Cr)A not only has a high proton conductivity of 1.27×10^{-1} S cm^{-1} at 100% RH and 80 °C but also maintains moderately high proton conductivity at a wide range of RH and temperature.

Developing clean and renewable energy solutions to move away from the burning of fossil fuels is receiving considerable attention[1]. Among the diverse range of advanced energy storage and conversion devices being explored to address these challenging energy and environment issues, proton exchange membrane fuel cells (PEMFCs) are considered to be very promising options due to their pre-eminent performance in terms of their high energy density, low pollutant emissions and mild operating conditions[2]. Although extensive research efforts have been pursued, the design of electrolyte materials with both high proton conductivity and stability for PEMFCs remains a challenge. The commonly used or explored electrolyte materials, such as Nafion[3,4] and its alternative polymers[5,6], porous inorganic/carbon materials[7,8] and inorganic/polymer composites[9,10], usually suffer from significantly reduced proton conductivity at low relative humidity (RH). The low water content could lead to the breaking of water-mediated hydrogen-bonding networks in these materials, thereby reducing the performance of the fuel cell[11]. Water content management has thus stood out as one of the key challenges in PEMFCs for a long time[12]. Technically, a humidification system can be introduced to preserve the minimum level of electrolyte hydration for high proton conductivity[13]; however, such additional components not only make the structure of PEMFCs more complex but also increase the cost[14], particularly in multi-cell stacks. Therefore, it is highly desirable to design and exploit a smart proton-conducting material that can self-adapt its structure under variable moisture levels to maintain hydrogen-bonding networks and thus to ensure high proton conductivity over a wide RH range.

Metal–organic frameworks (MOFs) have attracted extensive interest and undergone rapid development in the past two decades due to their designable and tunable structures and properties, as well as their potential applications in, for example, gas adsorption and separation[15–17], sensing[18] and energy-related applications[19,20]. For instance, it has been demonstrated that proton-conducting MOFs are potentially applicable in PEMFCs[21–24]. Since hydrogen-bonding networks can facilitate proton migration, the introduction of hydrophilic functional groups/entities into MOF structures can initiate the formation of continuous hydrogen-bonding networks and result in high proton conductivity[25,26]. Among the examined hydrophilic groups, the sulfonic acid group (–SO_3H) is one of the best, which can significantly augment the proton conductivity through its involvement in hydrogen-bonding networks and by providing proton donors[27]. MOFs have been categorized into three generations based on their structural and permanent porosity features[28]: the first generation of unstable MOFs have no permanent porosity when guest molecules are removed; the second generation of rigid MOFs (RMOFs) maintain their robust and porous frameworks during the material activation; and the third generation of flexible MOFs (FMOFs) can reversibly respond to external stimuli while maintaining framework integrity. Previously, the research on MOFs for proton conduction has been mainly focused on the RMOFs with the highest reported proton conductivity up to 10^{-2} S cm^{-1} at high RH[27,29–32]. However, the rigid pores within RMOFs cannot self-adapt themselves to respond to moisture changes, so the hydrogen-bonding networks formed under high humidity might break under low humidity, leading to low proton conductivity. FMOFs might provide the resolution to ensure high proton conductivity both at high and low humidity through the self-adaption of their structures under different moisture levels to maintain the hydrogen-bonding networks, but have rarely been explored[33].

[1]Beijing Key Laboratory for Green Catalysis and Separation and Department of Chemistry and Chemical Engineering, College of Environmental and Energy Engineering, Beijing University of Technology, Beijing 100124, China. [2]State Key Laboratory of Structural Chemistry, Fujian Institute of Research on the Structure of Matter, Chinese Academy of Sciences, Fuzhou, Fujian 350002, China. [3]NIST Center for Neutron Research, National Institute of Standards and Technology, Gaithersburg, Maryland 20899-6102, USA. [4]Fujian Provincial Key Laboratory of Polymer Materials, College of Materials Science and Engineering, Fujian Normal University, Fuzhou, Fujian 350007, China. [5]Department of Chemistry, University of Texas at San Antonio, One UTSA Circle, San Antonio, Texas 78249-0698, USA. *e-mail: jrli@bjut.edu.cn; banglin.chen@utsa.edu

To achieve a good performance under harsh operation conditions in fuel cells, the electrolyte materials also need to be chemically stable. As most MOFs are unstable in water, acidic and/or basic media[34,35], in practice, they cannot be utilized in PEMFCs even if they have high proton conductivity. Significant progress on the construction of chemically stable MOFs based on using highly charged metal ions and/or metal-containing secondary building units, such as $Zr_6O_4(OH)_4(CO_2)_{12}$ in Zr-MOFs and $M_3O(X)(CO_2)_6$ (M = Cr or Al and X = F, OH or Cl) in the MIL series of MOFs, has provided approaches to design and synthesize stable MOFs under harsh conditions[36,37].

In this work, we report a structurally flexible and chemically stable Cr(III)-based MOF, $Cr_3(\mu_3\text{-}O)(H_2O)_3(NDC(SO_3H_{5/6})_2)_3$ (BUT-8(Cr)A, BUT = Beijing University of Technology), constructed from a naphthalene-2,6-dicarboxylate organic linker decorated with rich sulfonic acid ($-SO_3H$) sites, 4,8-disulfonaphthalene-2,6-dicarboxylatlate ($NDC(SO_3H)_2^{2-}$) and $Cr_3O(OH)(CO_2)_6$ secondary building units. This MOF exhibits high proton conductivity up to 1.27×10^{-1} S cm^{-1} at 100% RH and 80 °C, and can also maintain moderately high proton conductivities under a wide range of RH and temperature.

Synthesis and structure

BUT-8(Cr) was firstly synthesized as a crystalline powder through the reaction of $H_2NDC(SO_3H)_2$ and $Cr(NO_3)_3\cdot9H_2O$ in *N,N*-dimethylformamide (DMF) in the presence of hydrofluoric acid under solvothermal conditions. Powder X-ray diffraction (PXRD) analysis and Le Bail refinement show that BUT-8(Cr) is isostructural to the Al(III) analogue (Supplementary Figs. 1b, 2a and 3a), BUT-8(Al), whose structure was characterized by single-crystal X-ray diffraction (single crystals of BUT-8(Cr) are too small for single-crystal X-ray diffraction analysis). In the structure of BUT-8(M) (M = Al or Cr), each $M_3(\mu_3\text{-}O)$ cluster is linked to six organic ligands to form a three-dimensional (3D) framework with 1D channels running along the crystallographic *c* axis, as well as bi-pyramidal cages with diameters of about 12 and 14 Å, respectively (Fig. 1a–c and Supplementary Fig. 4). This structure is similar to that of MIL-88C[38]. A high density of sulfonate groups are thus located on the channel surfaces of the framework. The O–O axis of the carboxylate groups can work like a 'knee cap', around which the metal clusters and the naphthyl groups can change their angular orientations through rotation, respectively, leading to overall structural flexibility[38] (Supplementary Fig. 5).

The elemental analysis and Fourier transform infrared (FT-IR) spectra further confirm the existence of sulfonate groups in the framework of BUT-8(Al) and BUT-8(Cr) (Supplementary Fig. 6). These studies also show the existence of $NH_2(CH_3)_2^+$ cations inside the pores, in situ formed through the decomposition of DMF during the synthesis[39]. The ion chromatography reveals that there is no elemental fluorine in BUT-8(Cr). Clearly, sulfonate groups in ligands have an anionic form in BUT-8(Cr) to maintain the charge balance of the whole framework, similar to that in MIL-101-SO_3H (ref. [40]). On the basis of these results, the formula for BUT-8(Cr) can be written as $Cr_3(\mu_3\text{-}O)(H_2O)_3(NDC(SO_3)_2)_3\cdot(NH_2(CH_3)_2^+)_5$.

The existence of sulfonate groups and $NH_2(CH_3)_2^+$ counter-ions in BUT-8(Cr) motivated us to pursue ion exchange with H^+ to obtain the $-SO_3H$-functionalized partner for proton conduction. The freshly made BUT-8(Cr) sample was immersed in 0.5 M of H_2SO_4 aqueous solution three times (24 h for each time, and the solid was collected for the next immersion) successively, and then thoroughly washed with water to give a new freshly made phase, which was further washed with methanol and dried under vacuum to give the dried phase of the MOF, denoted as BUT-8(Cr)A. The pores of BUT-8(Cr) with the diameter larger than 10 Å (Supplementary Fig. 4) could allow the $NH_2(CH_3)_2^+$ to freely pass through and to be exchanged to yield BUT-8(Cr)A. As a result, the FT-IR spectrum of BUT-8(Cr)A shows that the characteristic absorption peaks of $NH_2(CH_3)_2^+$ in BUT-8(Cr) disappeared, confirming its exchange

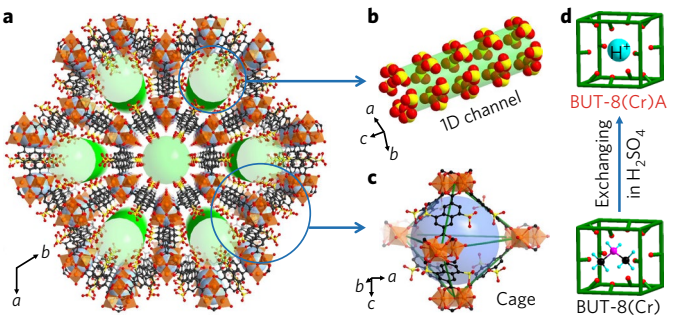

Fig. 1 | Structure of BUT-8(M) (M = Cr, Al) and the ion exchange in BUT-8(Cr). a, The crystal structure of BUT-8(M) viewed along the crystallographic *c* direction. **b**, A porous channel functionalized by sulfonate groups in BUT-8(M). **c**, A polyhedral cage unit in BUT-8(M). **d**, Schematic illustration of the ion exchange in BUT-8(Cr) to form BUT-8(Cr)A. The M (M = Cr, Al), O, S, N, H and C atoms are shown in orange, red, yellow, pink, turquoise and black, respectively. All hydrogen atoms (in **a** and **c**) and $NH_2(CH_3)_2^+$ cations (in **a**) are omitted for clarity.

by H^+ (Supplementary Fig. 6). The residual H_2SO_4 in the pores of BUT-8(Cr)A was removed, as supported by the fact that no further $BaSO_4$ precipitate was observed when a saturated $Ba(NO_3)_2$ aqueous solution was added to the supernatant of the BUT-8(Cr)A in water. The complete removal of H_2SO_4 and other guest molecules in the dried BUT-8(Cr)A sample has also been demonstrated by the thermogravimetry analysis (TGA) results for the samples after repeated activation treatments, which gave almost the same TGA curves (Supplementary Fig. 7). The elemental analysis results also prove that almost no N from $NH_2(CH_3)_2^+$ and redundant S from H_2SO_4 was left in this MOF. Thus, the formula for BUT-8(Cr)A can be illustrated as $Cr_3(\mu_3\text{-}O)(H_2O)_3(NDC(SO_3H_{5/6})_2)_3$. Furthermore, PXRD and Le Bail refinement reveal that BUT-8(Cr)A has an identical structure to BUT-8(Al) (Supplementary Figs. 1b, 2b and 3b).

Chemical stability and structural flexibility

As shown by PXRD, BUT-8(Cr)A was intact in aqueous solutions with a wide pH value range, even in 10 M sulfuric acid or concentrated hydrochloric acid for one week (Fig. 2a). Scanning electron microscopy and transmission electron microscopy reveal that both freshly made BUT-8(Cr)A and BUT-8(Cr) have an urchin-like particle morphology, composed of plentiful nanofibres that are 20~50 nm in diameter (Supplementary Fig. 8). After H_2SO_4 treatment, the resulting BUT-8(Cr)A sample has essentially the same morphology as that of BUT-8(Cr). Unlike BUT-8(Cr)A and BUT-8(Cr), the BUT-8(Al) sample, however, shows a much weaker and unidentifiable PXRD pattern after being immersed in water, implying that BUT-8(Al) is unstable in aqueous solution (Supplementary Fig. 9). Such different chemical stability has also been observed in the case of MIL-53(Cr) and MIL-53(Al) because of the different inertness or lability of $Cr_3(\mu_3\text{-}O)$ and $Al_3(\mu_3\text{-}O)$ clusters[41]. In addition, both BUT-8(Cr)A and BUT-8(Cr) are thermally stable up to ~280 °C, as confirmed by TGA and PXRD studies (Supplementary Figs. 10 and 11).

Furthermore, the PXRD studies show that the diffraction peaks of the freshly made BUT-8(Cr)A sample became broadened and shifted when it was exposed to an ambient environment with ~30% RH for about 40 min, suggesting a possible structural transformation (Supplementary Fig. 12). The colour of the sample also changed from green to light green simultaneously (Supplementary Fig. 13a). The dried BUT-8(Cr)A indeed had poor crystallinity with broadened diffraction peaks. However, the PXRD pattern and colour could be rapidly recovered in less than 2 min when the dried sample was treated with a flow of humid air (Supplementary Fig. 13b),

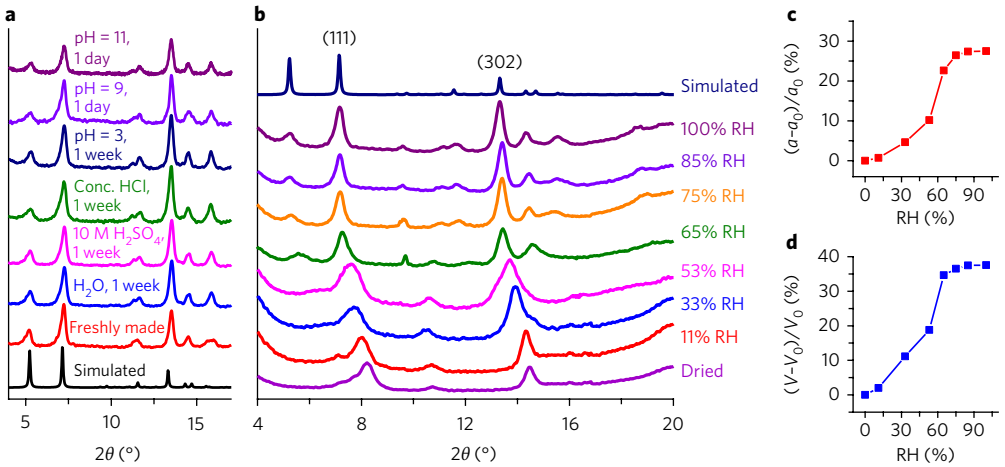

Fig. 2 | Chemical stability and structural flexibility of BUT-8(Cr)A. a, PXRD patterns of BUT-8(Cr)A after treatment in different acidic/basic aqueous solutions. **b**, Evolution of in situ PXRD patterns for BUT-8(Cr)A in different RHs at 25 °C. **c**,**d**, Dynamic structural transformation of BUT-8(Cr)A under various RHs (*a* and *V* are the cell parameters based on Le Bail refinements at different RHs, and a_0 and V_0 are the cell parameters for the dried BUT-8(Cr)A).

implying that the structural transformation is fast and reversible. The BUT-8(Cr)A sample thus demonstrates structural flexibility in response to humidity changes.

To explore the structural flexibility in detail, the evolution of the PXRD patterns of both the dried BUT-8(Cr)A and BUT-8(Cr) samples was traced in situ in different RHs at 25 °C (Fig. 2b and Supplementary Fig. 14). It was found that the two strongest peaks—the (111) and (302) planes—were gradually shifted to lower 2θ with increasing RH up to ~65% RH, showing a clear structural expansion. No obvious variation in the peak positions was observed after the RH exceeded ~65%. The changes in the lattice parameters in BUT-8(Cr)A were then refined on all diffraction patterns (Supplementary Fig. 15), and used to illustrate the structural transformation[42,43]. Consequently, the *a* axis expands continuously from the dried state with increased RH, up to 27.49% (Fig. 2c), while the *c* axis shrinks (Supplementary Fig. 16 and Supplementary Table 2). The overall change in the cell volume thus increases 37.58% from 12,508(26) Å^3 of the dried state to 17,209(81) Å^3 of the hydrated one (Fig. 2d and Supplementary Table 2). A similar structural expansion has previously been demonstrated for MIL-88, which has a similar structure to BUT-8(M) (M = Cr, Al)[38].

To confirm the water inclusion into the pores of BUT-8(Cr)A, water vapour adsorption of its dried sample was conducted at 25 °C. As shown in Supplementary Fig. 17a, the adsorption amounts increase with increasing water vapour pressure, up to 800 cm^3 g^{-1} at 100% RH, implying that the water molecules are absorbed into its pores. The observed increase in water uptake matches with the peak shift in Fig. 2b and the cell volume enlargement in Fig. 2d, especially the large peak shift and sharp increase near 65% RH. Similar phenomena have been observed in BUT-8(Cr) as well (Supplementary Figs. 14 and 18a). The water sorption isotherms of the two MOFs exhibit obvious hysteresis behaviour, being related to their flexible structures. Interestingly, BUT-8(Cr)A and BUT-8(Cr) are highly selective to take up water molecules, with uptakes of 35.7 and 26.1 mmol g^{-1}, respectively. However, their adsorptions toward the other gases examined (H_2, N_2, CO_2, C_2H_4, C_3H_6, C_2H_6, and C_3H_8) are low even at low temperatures, suggesting that these gas molecules might not have strong interactions with the frameworks to expand the pore spaces (Supplementary Figs. 17 and 18). The structural transformation of BUT-8(Cr)A can thus be attributed to the water adsorption in its pores under different RHs. The high polarity and abundant –SO_3H sites that have strong interactions with water molecules through hydrogen bonding enable this MOF to easily adsorb water molecules and thus to expand pore spaces[38].

Proton conductivity

To examine the proton conductivity of BUT-8(Cr)A, alternating current (a.c.) impedance was first carried out at 25 °C and different RHs (Supplementary Fig. 19). For comparison, BUT-8(Cr) and a representative RMOF, MIL-101-SO_3H (see Supplementary Fig. 20 for its characterization), were also examined. As shown in Fig. 3a and Supplementary Figs. 21 and 22, all three MOFs display good Debye semicircles or arcs, which can be fitted well with proposed equivalent circuits (Supplementary Figs. 23 and 24). It was found that the proton conductivity of BUT-8(Cr)A increases with increasing humidity and reaches 6.32×10^{-3} S cm^{-1} at 65% RH (with about 37 water molecules per formula (WMPF) adsorbed) (Fig. 3b), while the conductivity of BUT-8(Cr) reaches 1.12×10^{-3} S cm^{-1} at 65% RH. The proton conductivities of these two MOFs at this RH are higher than those of most reported proton-conducting MOFs, as summarized in Supplementary Table 3. For the rigid MIL-101-SO_3H, although adsorbing 34 WMPF at this RH, it represents a proton conductivity of only 5.92×10^{-4} S cm^{-1}, being about one order of magnitude lower than that of BUT-8(Cr)A. It is also interesting that the BUT-8(Cr)A and BUT-8(Cr) are still moderately proton conductive at a much lower RH of 11%, with conductivity of 4.19×10^{-6} and 5.75×10^{-7} S cm^{-1}, respectively, which are also significantly higher than that of MIL-101-SO_3H (5.84×10^{-9} S cm^{-1}) under the same RH. When the RH was increased to 100% at 25 °C, the proton conductivity of BUT-8(Cr)A and BUT-8(Cr) further increased to 7.61×10^{-2} and 1.50×10^{-2} S cm^{-1}, respectively (Fig. 3c and Supplementary Fig. 25), again higher than those of most reported proton-conducting MOFs. The increase in water content with increased RH obviously enhances the proton conductivities, which implies that protons primarily migrate through the inner pores of the MOFs[44]. Under the same conditions (100% RH and 25 °C), however, BUT-8(Cr)A and BUT-8(Cr) exhibit a much lower electronic conductivity of 5.10×10^{-8} and 1.28×10^{-8} S cm^{-1}, respectively, compared with their proton conductivities, suggesting that the two MOFs are strong proton conductors but basically electronic insulators.

Unlike MIL-101-SO_3H and other rigid MOFs, in which the proton conductivities are quasi-linearly correlated with the water content inside the pores[24,30,33] (Supplementary Fig. 22b), the proton conductivities of BUT-8(Cr)A and BUT-8(Cr) cannot be linearly correlated with the water content in the RH range of 11~65% (Fig. 3b and Supplementary Fig. 21b). As shown in Supplementary Fig. 26, initially, the proton conductivities of MIL-101-SO_3H, BUT-8(Cr)

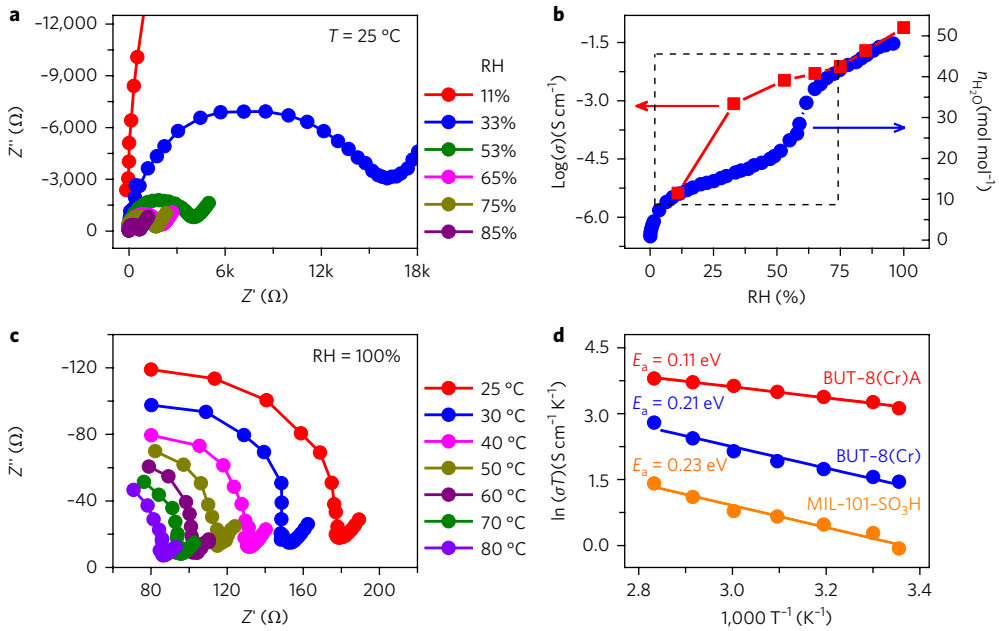

Fig. 3 | Proton conductivity of BUT-8(Cr)A. a, Humidity-dependent impedance plots of BUT-8(Cr)A at 11~85% RH. **b**, Log-scaled proton conductivity (red squares) of BUT-8(Cr)A at various RHs and the corresponding water adsorption isotherm at 25 °C (blue circles) (the area inside the dashed outline shows the distinct inconsistency between the proton conductivity and the water adsorption). **c**, Temperature-dependent impedance plots of BUT-8(Cr)A at 100% RH. **d**, Arrhenius plots of BUT-8(Cr)A, BUT-8(Cr) and MIL-101-SO_3H.

A and BUT-8(Cr) are all low at 11% RH. During the RH increase to ~65%, those of BUT-8(Cr)A and BUT-8(Cr) firstly increase rapidly, and then slowly reach stable high values (without rapid changes after about 50% RH), while the conductivity of MIL-101-SO_3H essentially increases linearly with the RH increase (Supplementary Fig. 22b). We propose that the observed unique water-content-dependent proton conduction of the two flexible MOFs could be attributed to the self-adaption of their frameworks to ensure proton transportation even at a comparatively low RH.

The proton conductivities for MIL-101-SO_3H, BUT-8(Cr)A and BUT-8(Cr) were further examined at elevated temperatures of up to 80 °C. As shown in Fig. 3c and Supplementary Fig. 25, at 100% RH, these MOFs show increased proton conductivities when the temperature increases, up to 1.16×10^{-2}, 4.63×10^{-2} and 1.27×10^{-1} S cm^{-1} at 80 °C for MIL-101-SO_3H, BUT-8(Cr) and BUT-8(Cr)A, respectively. Under this condition, the proton conductivity of BUT-8(Cr)A is about three times higher than that of BUT-8(Cr) and ten times that of MIL-101-SO_3H. To the best of our knowledge, the proton conductivity of BUT-8(Cr)A at 80 °C and 100% RH is the highest reported among the explored MOFs, and is also comparable to that of Nafion (Table 1).

Furthermore, both RH- and temperature-dependent conduction cyclic experiments were performed, giving well reproducible conductivities for the MOFs (Supplementary Figs. 27–32). At 100% RH, time-dependant measurements also show that BUT-8(Cr)A can retain its high proton conductivity at 25 and 80 °C for 100 and 40 h, respectively (Supplementary Figs. 33 and 34). PXRD studies also confirm the structural integrity of BUT-8(Cr)A after repeated

Table 1 | Comparison of proton conductivities in some reported MOFs (conductivity over 10^{-2} S cm^{-1}) and Nafion

Material	Proton conductivity (S cm−1)	RH and Temperature (°C)	Ref.
BUT-8(Cr)A	1.27×10^{-1}	100% and 80	This work
BUT-8(Cr)	4.63×10^{-2}	100% and 80	This work
MIL-101-SO_3H	1.16×10^{-2}	100% and 80	This work
Nafion	7.8×10^{-2}	100% and 25	Ref. [4]
UiO-66-$(SO_3H)_2$	8.4×10^{-2}	90% and 80	Ref. [27]
TfOH@MIL-101	8×10^{-2}	60% and 15	Ref. [49]
Fe-CAT-5	5×10^{-2}	98% and 25	Ref. [29]
$[(Me_2NH_2)_3(SO_4)]_2[Zn_2(ox)_3]$	4.2×10^{-2}	98% and 25	Ref. [30]
PCMOF10	3.55×10^{-2}	95% and 70	Ref. [31]
$H^+@Ni_2(dobdc)(H_2O)_2$	2.2×10^{-2}	95% and 80	Ref. [50]
PCMOF2½	2.1×10^{-2}	90% and 85	Ref. [32]
H_2SO_4@MIL-101	1.0×10^{-2}	0.13% and 150	Ref. [44]
H_3PO_4@MIL-101	1.0×10^{-2}	1.1% and 140	Ref. [44]

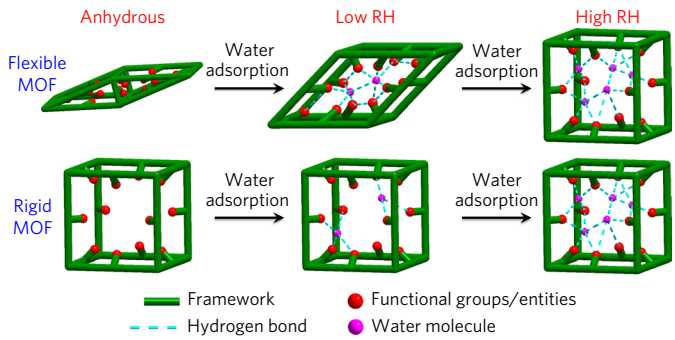

Fig. 4 | Proposed self-adaption mechanism. Schematic representation of the proposed mechanism, whereby structural changes are induced by water adsorption in flexible MOFs; at low RH the hydrogen-bonding networks in the pores are more uninterrupted in the flexible MOF than those in the rigid one due to the contracted pore size of the former, while at high RH successive hydrogen-bonding networks are present in both cases.

use (Supplementary Fig. 35). These results demonstrate the good stability of this MOF for proton conduction, as well as a lack of leaching of acid groups from the pores during repeated measurements. Simultaneously, we also observed that after three cycles of a.c. impedance measurements the BUT-8(Cr)A plate still has good contact with the silver electrode (Supplementary Fig. 30), suggesting good mechanical stability of the system.

Through a linear fit with equation (2) shown in the Methods, the evaluated activation energies (E_a) of BUT-8(Cr)A, BUT-8(Cr) and MIL-101-SO_3H are 0.11, 0.21 and 0.23 eV, respectively (Fig. 3d). The high proton conductivity and low activation energy of BUT-8(Cr)A confirm a fast-ion conducting behaviour, as rationalized on the basis of the Grotthuss mechanism[21,45]. This mechanism was also assessed by deuterium-related experiments. BUT-8(Cr)A and BUT-8(Cr) show reduced conductivities in a D_2O atmosphere (2.40×10^{-2} S cm^{-1} for BUT-8(Cr)A and 5.00×10^{-3} S cm^{-1} for BUT-8(Cr), Supplementary Figs. 36 and 37) compared with those in a H_2O atmosphere (7.61×10^{-2} S cm^{-1} for BUT-8(Cr)A and 1.50×10^{-2} S cm^{-1} for BUT-8(Cr)) at 25 °C. The reduced conductivities under the D_2O atmosphere are clearly related to the involvement of the deuterium atom, which is heavier than the proton[46–48]. Correspondingly, the low mobility of deuterium atoms also leads to higher activation energies (E_a) of 0.25 and 0.31 eV for BUT-8(Cr)A and BUT-8(Cr), respectively (Supplementary Figs. 38–41). These results support the aforementioned Grotthuss mechanism.

Discussion

BUT-8(Cr)A demonstrates excellent stability in water and strong acid. We suggest that its flexible nature enables it to respond to different water contents in its pores and maintain proton transportation even at a comparatively low RH. As well established, the excellent chemical stability can be attributed to the strong Cr–O bonds in the $Cr_3O(CO_2)_6$ units. The structural flexibility is related to the `knee cap' of the carboxylate functions as revealed in other flexible MOFs such as MIL-88 (ref. [38]). The high density of $-SO_3H$ has allowed very high proton conductivities in BUT-8(Cr)A, while the $NH_2(CH_3)_2^+$ can also donate protons for the high proton conductivity of BUT-8(Cr)[30]. More interestingly, they retain high proton conductivities even in a wide RH range. Such high proton conductivities at a wide range of RH could be attributed to the water-induced structural flexibility and the proposed self-adaption of the frameworks to maintain the hydrogen-bonding networks in their pores even at a comparatively low RH. This is unique among these two flexible MOFs, and has not been discovered before in rigid MOFs. In Fig. 4, we propose a model to rationalize the different water adsorption behaviours and thus RH-dependent proton conductivities of these two types of MOF. In both cases, the hydrogen-bonding networks would be largely broken down once the frameworks have been fully activated to remove the adsorbed water molecules. However, they should behave significantly different once the MOFs gradually take up water molecules: the FMOFs may be able to adjust and self-adapt the frameworks themselves, leading to the formation of a new and successive hydrogen-bonding network for proton transportation during the transition states from fully activated MOFs to fully hydrated ones. RMOFs may be less able to form successive hydrogen-bonding networks for proton transportation at low RH, which could only be recovered in the fully hydrated states.

In summary, we have demonstrated a chemically stable and structurally flexible MOF, BUT-8(Cr)A, with high proton conductivity in a wide RH range up to 1.27×10^{-1} S cm^{-1} at 80 °C and 100% RH. We propose that the high proton conductivity might be attributed to not only its hydrophilic pores functionalized by large numbers of $-SO_3H$ sites but also a water-content-dependent structural transformation of the framework, so-called framework 'self-adaption'. This work provides the promise of developing flexible MOFs with high proton conductivities at a wide temperature and humidity range, thus facilitating their potential applications in PEMFCs.

Methods

Materials. The commercial chemicals were purchased directly and used without further purification. Chromium(III) nitrate nonahydrate ($Cr(NO_3)_3{\cdot}9H_2O$), aluminium nitrate nonahydrate ($Al(NO_3)_3{\cdot}9H_2O$) and trifluoroacetic acid (TFA) were purchased from Alfa Aesar. 2-Sulfoterephthalic acid monosodium salt (H_2BDC-SO_3Na) and 2,6-naphthalenedicarboxylic acid (H_2NDC) were obtained from TCI. *N*,*N*'-dimethylformamide (DMF), hydrochloric acid, sulfuric acid, fuming sulfuric acid (20 wt% excess SO_3), hydrofluoric acid (47~51 wt%) and methanol were purchased from Sinopharm Chemical Reagent Co, Ltd.

Synthesis of $H_2NDC(SO_3H)_2$. The ligand, 4,8-disulfonyl-2,6-naphthalenedicarboxylic acid ($H_2NDC(SO_3H)_2$) was synthesized according to the method described in the literature[51]. Typically, 100 ml of fuming sulfuric acid was added to a 250 ml three-neck flask containing H_2NDC (30.00 g, 0.14 mol) under stirring. Then the reaction mixture was vigorously stirred at 140 °C for 24 h. After cooling down to room temperature, the mixture was dissolved in deionized water (50 ml), and then the target product, $H_2NDC(SO_3H)_2$, was precipitated using concentrated hydrochloric acid (200 ml). After collection by centrifugation and drying at 80 °C for 12 h, the obtained white power was again dissolved in deionized water (20 ml) and then precipitated with concentrated hydrochloric acid (100 ml) following a centrifugation process. This dissolution–precipitation process was repeated at least three times to ensure the residual H_2SO_4 was removed. Finally, the obtained $H_2NDC(SO_3H)_2$ was dried at 80 °C for 12 h.

Synthesis of BUT-8(Cr). $Cr(NO_3)_3{\cdot}9H_2O$ (400 mg, 1 mmol), $H_2NDC(SO_3H)_2$ (376 mg, 1 mmol), hydrofluoric acid (~47 wt% aqueous solution, 110 µl, 2.6×10^{-3} mmol) and DMF (6 ml) were charged in a 20 ml Teflon-lined stainless-steel autoclave. The autoclave was heated at 190 °C for 24 h and then cooled down to room temperature spontaneously. A mixture of green powder and large bright-green single crystals was collected through filtration. The green powder of the target MOF, BUT-8(Cr), was separated from the mixture by following a simple procedure: the resulting mixture was stirred in DMF and then left for about one minute to allow all of the single crystals to settle; then, the suspension with the green powder was carefully sucked out using a straw. The green solid was then collected from the suspension by centrifugation and washed with DMF (50 ml). The obtained solid was further soaked in hot DMF (100 ml, 80 °C) for 24 h and then collected and washed three times with DMF. The DMF-washed sample was further soaked in water (200 ml) for 24 h at room temperature and then washed three times with fresh water to obtain the freshly made BUT-8(Cr) sample. Finally, the freshly made product was washed with methanol and dried under a vacuum at 60 °C for 12 h to obtain dried BUT-8(Cr). Elemental analysis for BUT-8(Cr), $Cr_3(\mu_3\text{-}O)(H_2O)_3(NDC(SO_3)_2)_3(NH_2(CH_3)_2^+)_5$ (FW: 1573.33): calculated (%): Cr, 9.91; C, 35.12; H, 3.72; N, 4.45, and S, 12.20. Found (%): Cr, 9.60 (ICP); C, 34.92; H, 3.43; N, 4.72; and S, 12.06. For the PXRD pattern of the freshly made BUT-8(Cr), FT-IR spectrum and thermogravimetry analysis (TGA) curve for dried BUT-8(Cr), see Supplementary Figs. 1b, 6 and 10, respectively).

Synthesis of BUT-8(Cr)A. To obtain BUT-8(Cr)A, the freshly made BUT-8(Cr) sample (500 mg) was washed three times with 0.5 M sulfuric acid aqueous solution (200 ml), and then soaked in 0.5 M sulfuric acid aqueous solution (100 ml) for 24 h. This impregnation process was repeated at least three times. Then, the sample was

collected through centrifugation, and washed with water three times. The obtained sample was alternately soaked three times in water (100 ml each time, for 24 h) and two times in methanol (100 ml each time, for 12 h). Finally, the sample was washed with fresh water to obtain the freshly made BUT-8(Cr)A sample, which was further washed with methanol and dried at 60 °C under a vacuum for 24 h to obtain dried BUT-8(Cr)A. Elemental analysis for BUT-8(Cr)A, $Cr_3(\mu_3\text{-}O)(H_2O)_3(NDC(SO_3H_{5/6})_2)_3$ (FW: 1347.91): calculated (%): Cr, 11.57; C, 32.07; H, 1.72; N, 0.00, and S, 14.27. Found (%): Cr, 11.20 (ICP); C, 31.25; H, 2.24; N, 0.12, and S, 14.08. For PXRD patterns (including the Le Bail refinement) of freshly made BUT-8(Cr)A, FT-IR spectrum and TGA curve of dried BUT-8(Cr)A, see Supplementary Figs. 1b, 2b, 6 and 10, respectively.

Synthesis of BUT-8(Al) single crystals. $Al(NO_3)_3{\cdot}9H_2O$ (19 mg, 0.05 mmol), $H_2NDC(SO_3H)_2$ (19 mg, 0.05 mmol) and trifluoroacetic acid (TFA, 0.2 ml, 2.69 mmol) were dissolved in 2 ml DMF. The mixture was transferred to a 4 ml vial and then sealed in a 20 ml Teflon-lined stainless-steel autoclave. The autoclave was heated at 150 °C for 72 h and then cooled down naturally to room temperature. Block-shaped colourless single crystals (as the freshly made sample) were obtained through filtration. For general characterization, the obtained sample was washed with DMF and acetone in sequence, and dried at 60 °C under a vacuum for 24 h. For the PXRD pattern of the freshly made BUT-8(Al) and the FT-IR spectrum of dried BUT-8(Al), see Supplementary Figs. 1 and 6, respectively.

Synthesis of MIL-101-SO_3H. MIL-101-SO_3H was synthesized by following a reported procedure[52]. $Cr(NO_3)_3{\cdot}9H_2O$ (2.00 g, 5 mmol), $H_2BDC\text{-}SO_3Na$ (2.70 g, 10 mmol), deionized water (30 ml) and hydrofluoric acid (~47wt%, 0.3 g) were mixed in a 100 ml Teflon-lined stainless-steel autoclave and then heated at 190 °C for 24 h. After the reaction system was cooled down to room temperature, the green powder was collected by centrifugation and washed with deionized water five times. Finally, the product was collected and dried in air at 100 °C for 12 h. For the PXRD pattern of the freshly made MIL-101-SO_3H, see Supplementary Fig. 20a.

Single-crystal X-ray diffraction. The diffraction data for BUT-8(Al) were collected in a Rigaku Supernova CCD (charge-coupled device) diffractometer equipped with mirror-monochromatic-enhanced Cu-Kα radiation ($\lambda = 1.54184$ Å) at 100 K. The data set was corrected by empirical absorption correction using spherical harmonics, implemented in the SCALE3 ABSPACK scaling algorithm. The structure was solved by direct methods and refined by full-matrix least-squares on F^2 with anisotropic displacement by using the SHELXTL software package[53]. Non-hydrogen atoms were refined with anisotropic displacement parameters during the final cycle. Hydrogen atoms of ligands were calculated in ideal positions with isotropic displacement parameters. There is a large solvent-accessible pore volume in the structure, which is occupied by highly disordered solvent molecules and $NH_2(CH_3)_2^+$ cations. No satisfactory models for these entities could be achieved due to their severe crystallographic disorder, and therefore the SQUEEZE program implemented in PLATON[54] was used to remove the electron densities of these disordered species. Thus, all electron densities from $NH_2(CH_3)_2^+$ cations and free solvent molecules have been `squeezed' out. The details for the crystal data and structural refinement can be found in Supplementary Table 1 and Supplementary Data 1.

Proton conductivity measurement. Typically, the MOF powder was first pressed to form a plate and then measured by a.c impedance in an electrochemical workstation at controlled humidity and temperature. In detail, as shown in Supplementary Fig. 19, the given MOF powder (about 90 mg) was pressed at 1,000 kg cm^{-2} pressure for 3 min to make a plate (about 0.2 × 0.4 × 1.0 cm^3). Both sides of the plate were attached to silver wires with silver paste and then sealed in a home-made, double-walled glass chamber (30 cm in height and 5 cm in diameter) by a rubber plug. Meanwhile, a K-type thermocouple was also sealed and located close to the sample plate in the glass chamber to monitor the temperature of the system. The RH was controlled by saturated salt aqueous solutions as reported previously[55,56]. The impedance measurements were carried out by using a Zennium electrochemical workstation with tuned frequency range from 1 Hz to 4 MHz and an alternating potential of 100 mV. The proton conductivity (σ, S cm^{-1}) of the sample was estimated by using the equation:

$$\sigma = L/(RWd) \quad (1)$$

where L (1.0 cm) is the length, W (0.4 cm) is the width and d (cm) is the thickness of the measured plate; R (Ω) is the measured impedance.

To obtain the electrical conductivity at 25 °C and 100% RH, the electronic resistance (R (Ω)), which follows Ohm's law, is first calculated by taking the ratio between electrical current (I) and voltage (V) obtained by using the aforementioned device and the two-probe method (quasi-four-probe method) under direct current (d.c.). Then the electrical conductivity can be calculated by using equation (1)[57].

The activation energy (E_a) is calculated by using the conductivity data between 25 and 80 °C at 100% RH with the Arrhenius equation:

$$\ln(\sigma_T) = \ln A - E_a/\left(k_{B_T}\right) \quad (2)$$

where k_B and A are the Boltzmann constant and the pre-exponential factor, respectively.

Other physical measurements. The powder X-ray diffraction (PXRD) patterns were recorded on a Bruker D8 Advance Diffractometer by using Cu-Kα radiation ($\lambda = 1.541874$ Å). To investigate the in situ PXRD evolution of BUT-8(Cr) and BUT-8(Cr)A under changed humidity, the sample was first sealed in the furnace of a diffractometer and then humid N_2 gas was allowed to flow through to control the RH. The RH was regulated by bubbling N_2 gas through various saturated salt solutions (LiCl, ~11% RH; $MgCl_2$, ~33% RH; $Mg(NO_3)_2$, ~53% RH; $NaNO_2$, ~65% RH; NaCl, ~75% RH; and KCl, ~85% RH) and deionized water (100% RH), respectively. A Micrometrics ASAP 2020 Surface Characterization Analyzer was used to measure all of the gas and water vapour adsorption/desorption isotherms. A SHIMADZU IR Affinity-1 instrument was used for measuring FT-IR spectra. Elemental analysis was performed by a vario EL cube (Elementar). Inductively coupled plasma–optical emission spectrometer (ICP–OES) data were collected on a Thermo iCAP-6300. TGA experiments were performed on a TG/DTA6300 (SII) thermal analyser with heating from 25 to 700 °C (5 °C min^{-1}) in a nitrogen atmosphere. A few milligrams of BUT-8(Cr)A and BUT-8(Cr) were also heated in the TG/DTA6300 (SII) thermal analyser at 280 °C for 10 min to test their thermal stability. The fluorine content was detected by ion chromatography (Dionex DX-500).

Data availability. The X-ray crystallographic data for BUT-8(Al) have been deposited at the Cambridge Crystallographic Data Centre (CCDC), under deposition number CCDC 1564881. These data can be obtained free of charge from the CCDC via www.ccdc.cam.ac.uk. Crystallographic information for BUT-8(Al) can also be found in Supplementary Data 1. All other relevant data supporting the findings of this study are available from the corresponding authors on request.

Received: 8 February 2017; Accepted: 11 September 2017;
Published online: 16 October 2017

References

1. *Fuel Cell Technologies Office Multi-Year Research, Development, and Demonstration Plan* Section 1.0 (US DOE, 2016).
2. Barbir, F. *PEM Fuel Cells: Theory and Practice*. (Elsevier Academic Press, New York, 2005).
3. Mauritz, K. A. & Moore, R. B. State of understanding of Nafion. *Chem. Rev.* **104**, 4535–4585 (2004).
4. Sone, Y., Ekdunge, P. & Simonsson, D. Proton conductivity of Nafion 117 as measured by a four-electrode AC impedance method. *J. Electrochem. Soc.* **143**, 1254–1259 (1996).
5. Hickner, M. A. et al. Alternative polymer systems for proton exchange membranes (PEMs). *Chem. Rev.* **104**, 4587–4611 (2004).
6. Sel, O. et al. Original fuel-cell membranes from crosslinked terpolymers via a "sol-gel" strategy. *Adv. Funct. Mater.* **20**, 1090–1098 (2010).
7. Vichi, F. M., Tejedor-Tejedor, M. I. & Anderson, M. A. Effect of pore-wall chemistry on proton conductivity in mesoporous titanium dioxide. *Chem. Mater.* **12**, 1762–1770 (2000).
8. Karim, M. R. et al. Graphene oxide nanosheet with high proton conductivity. *J. Am. Chem. Soc.* **135**, 8097–8100 (2013).
9. Di Vona, M. L. et al. SPEEK/PPSU-based organic-inorganic membranes: proton conducting electrolytes in anhydrous and wet environments. *J. Membr. Sci.* **279**, 186–191 (2006).
10. Chalkova, E., Fedkin, M. V., Wesolowski, D. J. & Lvov, S. N. Effect of TiO_2 surface properties on performance of Nafion-based composite membranes in high temperature and low relative humidity PEM fuel cells. *J. Electrochem. Soc.* **152**, A1742–A1747 (2005).
11. Einsla, M. L. et al. Toward improved conductivity of sulfonated aromatic proton exchange membranes at low relative humidity. *Chem. Mater.* **20**, 5636–5642 (2008).
12. Nguyen, T. V. & White, R. E. A water and heat management model for proton-exchange-membrane fuel cells. *J. Electrochem. Soc.* **140**, 2178–2186 (1993).
13. Ahluwalia, R. K. et al. Performance of a cross-flow humidifier with a high flux water vapor transport membrane. *J. Power Sources* **291**, 225–238 (2015).
14. Kim, S. Y., Kim, S. & Park, M. J. Enhanced proton transport in nanostructured polymer electrolyte/ionic liquid membranes under water-free conditions. *Nat. Commun.* **1**, 88 (2010).
15. Sumida, K. et al. Carbon dioxide capture in metal-organic frameworks. *Chem. Rev.* **112**, 724–781 (2012).
16. Denny, M. S. Jr, Moreton, J. C., Benz, L. & Cohen, S. M. Metal-organic frameworks for membrane-based separations. *Nat. Rev. Mater.* **1**, 16078 (2016).
17. Schoedel, A., Ji, Z. & Yaghi, O. M. The role of metal-organic frameworks in a carbon-neutral energy cycle. *Nat. Energy* **1**, 16034 (2016).
18. Kreno, L. E. et al. Metal-organic framework materials as chemical sensors. *Chem. Rev.* **112**, 1105–1125 (2012).

19. Bai, S., Liu, X., Zhu, K., Wu, S. & Zhou, H. Metal-organic framework-based separator for lithium-sulfur batteries. *Nat. Energy* **1**, 16094 (2016).
20. Zhao, S. et al. Ultrathin metal-organic framework nanosheets for electrocatalytic oxygen evolution. *Nat. Energy* **1**, 16184 (2016).
21. Ramaswamy, P., Wong, N. E. & Shimizu, G. K. H. MOFs as proton conductors- challenges and opportunities. *Chem. Soc. Rev.* **43**, 5913–5932 (2014).
22. Horike, S., Umeyama, D. & Kitagawa, S. Ion conductivity and transport by porous coordination polymers and metal-organic frameworks. *Acc. Chem. Res.* **46**, 2376–2384 (2013).
23. Sahoo, S. C., Kundu, T. & Banerjee, R. Helical water chain mediated proton conductivity in homochiral metal-organic frameworks with unprecedented zeolitic unh-topology. *J. Am. Chem. Soc.* **133**, 17950–17958 (2011).
24. Sen, S., Nair, N. N., Yamada, T., Kitagawa, H. & Bharadwaj, P. K. High proton conductivity by a metal-organic framework incorporating Zn_8O clusters with aligned imidazolium groups decorating the channels. *J. Am. Chem. Soc.* **134**, 19432–19437 (2012).
25. Yoon, M., Suh, K., Natarajan, S. & Kim, K. Proton conduction in metal-organic frameworks and related modularly built porous solids. *Angew. Chem. Int. Ed.* **52**, 2688–2700 (2013).
26. Shigematsu, A., Yamada, T. & Kitagawa, H. Wide control of proton conductivity in porous coordination polymers. *J. Am. Chem. Soc.* **133**, 2034–2036 (2011).
27. Phang, W. J. et al. Superprotonic conductivity of a UiO-66 framework functionalized with sulfonic acid groups by facile postsynthetic oxidation. *Angew. Chem. Int. Ed.* **54**, 5142–5146 (2015).
28. Horike, S., Shimomura, S. & Kitagawa, S. Soft porous crystals. *Nat. Chem.* **1**, 695–704 (2009).
29. Nguyen, N. T. T. et al. Three-dimensional metal-catecholate frameworks and their ultrahigh proton conductivity. *J. Am. Chem. Soc.* **137**, 15394–15397 (2015).
30. Nagarkar, S. S., Unni, S. M., Sharma, A., Kurungot, S. & Ghosh, S. K. Two-in-one: inherent anhydrous and water-assisted high proton conduction in a 3D metal-organic framework. *Angew. Chem. Int. Ed.* **53**, 2638–2642 (2014).
31. Ramaswamy, P., Wong, N. E., Gelfand, B. S. & Shimizu, G. K. H. A water stable magnesium MOF that conducts protons over 10^{-2} S cm^{-1}. *J. Am. Chem. Soc.* **137**, 7640–7643 (2015).
32. Kim, S., Dawson, K. W., Gelfand, B. S., Taylor, J. M. & Shimizu, G. K. H. Enhancing proton conduction in a metal-organic framework by isomorphous ligand replacement. *J. Am. Chem. Soc.* **135**, 963–966 (2013).
33. Colodrero, R. M. P. et al. High proton conductivity in a flexible, cross-linked, ultramicroporous magnesium tetraphosphonate hybrid framework. *Inorg. Chem.* **51**, 7689–7698 (2012).
34. Burtch, N. C., Jasuja, H. & Walton, K. S. Water stability and adsorption in metal-organic frameworks. *Chem. Rev.* **114**, 10575–10612 (2014).
35. Howarth, A. J. et al. Chemical, thermal and mechanical stabilities of metal-organic frameworks. *Nat. Rev. Mater.* **1**, 15018–15031 (2016).
36. Wang, C., Liu, X., Demir, N. K., Chen, J. P. & Li, K. Applications of water stable metal-organic frameworks. *Chem. Soc. Rev.* **45**, 5107–5134 (2016).
37. Bai, Y. et al. Zr-based metal-organic frameworks: design, synthesis, structure, and applications. *Chem. Soc. Rev.* **45**, 2327–2367 (2016).
38. Serre, C. et al. Role of solvent-host interactions that lead to very large swelling of hybrid frameworks. *Science* **315**, 1828–1831 (2007).
39. Nouar, F., Eckert, J., Eubank, J. F., Forster, P. & Eddaoudi, M. Zeolite-like metal-organic frameworks (ZMOFs) as hydrogen storage platform: lithium and magnesium ion-exchange and H_2-(rho-ZMOF) interaction studies. *J. Am. Chem. Soc.* **131**, 2864–2870 (2009).
40. Akiyama, G., Matsuda, R., Sato, H., Takata, M. & Kitagawa, S. Cellulose hydrolysis by a new porous coordination polymer decorated with sulfonic acid functional groups. *Adv. Mater.* **23**, 3294–3297 (2011).
41. Kang, J., Khan, N. A., Haque, E. & Jhung, S. H. Chemical and thermal stability of isotypic metal-organic frameworks: effect of metal ions. *Chem. Eur. J.* **17**, 6437–6442 (2011).
42. Grimaud, A. et al. Activation of surface oxygen sites on an iridium-based model catalyst for the oxygen evolution reaction. *Nat. Energy* **2**, 16189 (2017).
43. Rangasamy, E. et al. An iodide-based $Li_7P_2S_8I$ superionic conductor. *J. Am. Chem. Soc.* **137**, 1384–1387 (2015).
44. Ponomareva, V. G. et al. Imparting high proton conductivity to a metal-organic framework material by controlled acid impregnation. *J. Am. Chem. Soc.* **134**, 15640–15643 (2012).
45. Zheng, N., Bu, X. & Feng, P. Synthetic design of crystalline inorganic chalcogenides exhibiting fast-ion conductivity. *Nature* **426**, 428–432 (2003).
46. Umeyama, D., Horike, S., Inukai, M. & Kitagawa, S. Integration of intrinsic proton conduction and guest-accessible nanospace into a coordination polymer. *J. Am. Chem. Soc.* **135**, 11345–11350 (2013).
47. Xu, H., Tao, S. & Jiang, D. Proton conduction in crystalline and porous covalent organic frameworks. *Nat. Mater.* **15**, 722 (2016).
48. Kang, D. W. et al. Cost-effective, high-performance porous-organic-polymer conductors functionalized with sulfonic acid groups by direct postsynthetic substitution. *Angew. Chem. Int. Ed.* **55**, 16357–16360 (2016).
49. Dybtsev, D. N. et al. High proton conductivity and spectroscopic investigations of metal-organic framework materials impregnated by strong acids. *ACS Appl. Mater. Inter.* **6**, 5161–5167 (2014).
50. Phang, W. J. et al. pH-dependent proton conducting behavior in a metal-organic framework material. *Angew. Chem. Int. Ed.* **53**, 8383–8387 (2014).
51. Papadaki, I., Malliakas, C. D., Bakas, T. & Trikalitis, P. N. Molecular supertetrahedron decorated with exposed sulfonate groups built from mixed-valence tetranuclear $Fe_3^{3+}Fe^{2+}(\mu_3\text{-}O)(\mu_3\text{-}SO_4)_3(CO_2)_3$ clusters. *Inorg. Chem.* **48**, 9968–9970 (2009).
52. Juan-Alcaniz, J. et al. Towards acid MOFs catalytic performance of sulfonic acid functionalized architectures. *J. Catal. Sci. Technol.* **3**, 2311–2318 (2013).
53. Sheldrick, G. M. SHELXTL NT Version 5.1, Program for Solution and Refinement of Crystal Structures. (University of Göttingen, Germany, 1997).
54. Spek, A. L. Single-crystal structure validation with the program PLATON. *J. Appl. Cryst.* **36**, 7–13 (2003).
55. Taylor, J. M. et al. Facile proton conduction via ordered water molecules in a phosphonate metal-organic framework. *J. Am. Chem. Soc.* **132**, 14055–14057 (2010).
56. Liang, X. et al. From metal-organic framework (MOF) to MOF-polymer composite membrane: enhancement of low-humidity proton conductivity. *Chem. Sci.* **4**, 983–992 (2013).
57. Sun, L., Campbell, M. G. & Dincă, M. Electrically conductive porous metal-organic frameworks. *Angew. Chem. Int. Ed.* **55**, 3566–3579 (2016).

Acknowledgements

This work was financially supported by the National Natural Science Fund for Innovative Research Groups (51621003), the Natural Science Foundation of China (No. 21576006, 21606006), the Importation and Development of High-Caliber Talents Project of Beijing Municipal Institutions (CIT&TCD20150309) and the Welch Foundation (AX-1730).

Author contributions

J.-R.L. and F.Y. conceived the research idea and designed the experiments. F.Y. performed most of the experiments and analysed data. B.W. participated in the structural determination of MOFs. H.Z. participated in the preparation of MOFs. Y.D. participated in the proton conduction measurement. H.W. and W.Z. performed the PXRD and Le Bail refinements. J.-R.L., B.C., H.W., W.Z., G.X. and F.Y. discussed and co-wrote the paper. All authors discussed the results and commented on the manuscript.

Competing interests

The authors declare no competing financial interests.

Additional information

Supplementary information is available for this paper at https://doi.org/10.1038/s41560-017-0018-7.

Reprints and permissions information is available at www.nature.com/reprints.

Correspondence and requests for materials should be addressed to J.-R.L. or B.C.

Publisher's note: Springer Nature remains neutral with regard to jurisdictional claims in published maps and institutional affiliations.